Hindawi
Geofluids
Volume 2020, Article ID 8837962, 10 pages
https://doi.org/10.1155/2020/8837962

Research Article

Experimental Study on the Gas Flow Characteristics and Pressure Relief Gas Drainage Effect under Different Unloading Stress Paths

Chaolin Zhang[1,2] **Jiang Xu**[3] **Enyuan Wang**[1,2] **and Shoujian Peng**[3]

[1]*Key Laboratory of Gas and Fire Control for Coal Mines (China University of Mining and Technology), Ministry of Education, Xuzhou, Jiangsu 221116, China*
[2]*School of Safety Engineering, China University of Mining and Technology, Xuzhou, Jiangsu 221116, China*
[3]*State Key Laboratory of Coal Mine Disaster Dynamics and Control, Chongqing University, Chongqing 400030, China*

Correspondence should be addressed to Chaolin Zhang; chaolinzhang@cumt.edu.cn

Received 12 June 2020; Revised 5 July 2020; Accepted 8 July 2020; Published 12 August 2020

Academic Editor: Jingmin Xu

Coal seam gas is a critical substance because it can be a source of a large quantity of clean energy as well as a dangerous source of risk. A pressure relief gas drainage is an effective and widely used method for coal seam gas recovery and gas disaster control in coal mines. A series of pressure relief gas drainage experiments were conducted using large-scale coal samples under different unloading stress paths in this study to explore the unloading stress paths. From the experimental results, the dynamic evolutions of gas pressure, coal temperature, and gas production were analyzed. The trends of gas pressure and coal temperature during pressure relief gas drainage were similar: dropping rapidly first and then slowly with time. Correspondingly, gas production was fast in the early stage of pressure relief gas drainage and became stable thereafter. Meanwhile, gas flow characteristics were significantly affected by the unloading stress paths. Gas pressure and coal temperature had the maximum descent by unloading stress in three directions simultaneously, and the unloading stress of the Z direction had the minimal impact when only unloading in one direction of stress. However, the influence of unloading stress paths on gas production was complex and time dependent. The difference coefficient parameter was proposed to characterize the influence degree of unloading stress paths on the pressure relief gas drainage effect. Eventually, the selection of unloading stress path under different situations was discussed based on time, which is expected to provide the basis for pressure relief gas drainage.

1. Introduction

With the rapid industrialization development, the consumption of the fossil fuel that is a nonrenewable resource is increasing day by day. Coal seam gas is an accessory product of the coalification process, which mainly produces methane and low concentrations of carbon dioxide, nitrogen, hydrogen sulfide, sulfur dioxide, and heavier hydrocarbons [1–5]. The total world reserves of coal seam gas are estimated to be 262 trillion m^3, and it has received increasing interest from many countries including USA, Australia, Canada, and China [6, 7]. However, coal seam gas is a double-edged sword, which cannot only be a source of high quality clean energy in large quantities but also is a dangerous source of risk in coal mines [8–10]. Coal seam gas with high pressure and high content can easily induce coal-gas dynamic disasters, e.g., coal and gas outburst, and coal gas explosion [11–13]. Therefore, high-efficient gas drainage is very important for the safety production of the coal mine.

The reserves of China's coal seam gas with a burial depth of below 2000 m are estimated to be 36.8 trillion m^3, which is more than that of shale and tight gas [14, 15]. However, coal seams in China are characterized by low gas saturation, low permeability, low reservoir pressure, and a relatively high metamorphic grade [16, 17]. For example, the permeability of most coal seams in China ranges from 10^{-4} to 10^{-1} mD, which is three to four orders of magnitude lower than that of most countries around the world [18, 19]. To improve coal seam gas recovery and control gas disasters, the technology of pressure relief gas drainage is proposed, which is widely used for the low permeability coal seam in China. Yuan expounded the theory and technology of pressure relief gas

drainage systematically and demonstrated the successful application of pressure relief gas drainage in Huainan coalfield in 1998 resulting to an increase in gas production from 10 million m^3 to 2500 million m^3 in ten years [20]. Subsequently, increased in-depth research has been carried out on pressure relief gas drainage technology.

Zhang et al. explored the effect of gas pressure on gas permeability during pressure relief gas drainage and found that permeability and its sensitivity to gas pressure decreased with increasing effective stress or external stress [21, 22]. Yin et al. carried conducted a series of experiments to study the mining-induced mechanical behavior, gas permeability, and acoustic emission evolution of coal under triaxial loading and unloading conditions [23, 24]. Chen et al. studied the stress-strain relationship and its influence on permeability during the confining pressure stress unloaded by X-ray computerized tomography (CT) scanning [25]. Wang et al. concluded that the permeability and gas production can be improved by imposing effective loads on original coal seams through mining speed control during pressure relief gas drainage [26]. Shang et al. compared the pressure relief gas drainage effect by surface well drilling and the use of net-like penetrating boreholes (NPB) in Panyi Coal Mine, and their findings indicated that the average gas extraction concentration and average extraction purity of surface wells were higher than those of NPB by approximately 124.4% and 64.7%, respectively [27].

Most of the aforementioned studies are focused on the permeability evolution of coal under different unloading stress paths, and the coal samples used are small-scale making it difficult to study the parameter variation inside the coal and the drainage effect. Therefore, a series of pressure relief gas drainage experiments using large-scale coal samples under different unloading stress paths were conducted to explore the selection of unloading stress paths in this study considering the long term, high cost, and poor repeatability of pressure relief gas drainage tests in coal mine site.

2. Experimental Methods

2.1. Laboratory Device. The experiments of pressure relief gas drainage under different unloading stress paths are carried out using a large-scale multifunctional (LSMF) device. The LSMF device can simulate gas flow experiments (e.g., coal bed methane (CBM) drainage, carbon dioxide sequestration, carbon dioxide-enhanced CBM recovery (CO_2-ECBM)), and gas outburst disasters in laboratory that is described amply in Zhang et al. [28]. The LSMF device is comprised of a coal specimen box, a true triaxial loading system, a fast coal uncovering system, a gas flow system, a data acquisition system, and a specimen shaping system. The effective space of the coal specimen box is 1050 mm × 400 mm × 400 mm. The true triaxial loading system has nine sets of loading plates at three directions of the coal specimen box, which can be servocontrolled independently to realize different loading and unloading paths.

2.2. Sample Preparation. The experimental coal is taken from Jinjia Coal mine, which is located at the border of Guizhou and Yunnan provinces of China. Western Guizhou and Eastern Yunnan are the largest coal-producing region in South China and has a potential for high CBM yield [29]. The reconstructed coal sample is used in this study considering the difficulty to gain a large-scale raw coal, and the preparation of coal sample includes sampling, pressing, screening, and shaping [30]. The coal sample is divided into four layers and every layer is pressed for 1 h under a shaping stress of 7.5 MPa [15]. During the shaping stage, the gas drainage boreholes numbered I and II, the gas pressure sensors numbered *P*1-*P*40, and the temperature sensors numbered *T*1-*T*7 are fixed inside the coal sample as shown in Figure 1. The length of the boreholes is 330 mm and consists of the drainage section (the red part, 160 mm in length) and the sealing section (the blue part, 170 mm in length).

2.3. Experimental Design. The variables considered in the experiments are the unloading stress paths as shown in Figure 2. The initial stress in three directions (i.e., *X* direction, *Y* direction, and *Z* direction) is all 4.0 MPa. The stress is produced by unloading through different paths after the coal sample is saturated with a pore pressure of 1 MPa and the unloading stress rate is 2 MPa/min. The gas drainage experiment with the unloading stress path of *OA* is carried out first to study the drainage effect when the stress in the three directions is unloaded at the same time. The valves in the gas outlet are opened to start the gas drainage process while σ_X, σ_Y, and σ_Z decline to 0.1 MPa. The experimental parameters of gas pressure, temperature, and gas flow rate are recorded automatically until the end. To compare the gas drainage effect under the different unloading stress paths, the gas drainage experiments with the unloading stress paths of OB, OC, and OD are conducted in turn. During the unloading stress path of OB, σ_X drops to 0.1 MPa with AN unloading rate of 2 MPa/min while σ_Y and σ_Z remain unchanged at 4.0 MPa. In addition, σ_Y drops to 0.1 MPa during the unloading stress path of OC and σ_Z drops to 0.1 MPa during the unloading stress path of OD.

3. Results and Discussion

3.1. Gas Drainage Effect with Stress Unloaded in Three Directions. Figure 3 shows the dynamic evolution of gas pressure with the unloading stress path of OA. The linear distance between the four gas pressure sensors (*P*3, *P*4, *P*5, and *P*6) and the borehole is 280 mm. As shown in Figure 3(a), the gas pressure curves of four sensors are almost coincident, which decline quickly at first and then drop slowly. The gas pressure drops from 1.0 MPa to 0.03 MPa after 8 h of gas drainage. The gas pressure sensors of *P*13, *P*14, *P*15, and *P*16 are fixed near the outer wall of borehole. However, the pressure evolution trend of four sensors shows significant differences. The sensor of *P*15 is located near the middle of the drainage section of borehole, and *P*15 gas pressure drops faster than that of the other three sensors. The sensors of *P*13 and *P*14 were located near the sealing part of THE borehole, and the gas pressure decreases at the slowest rate. The sensor of *P*16 is located at the front of the drainage section of borehole, and the gas pressure descent rate is

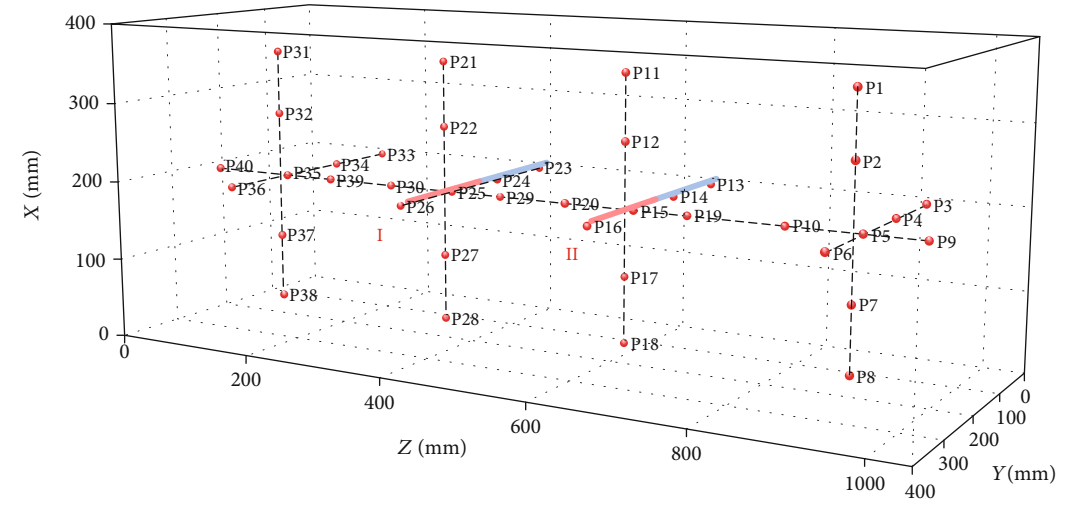

(a) Gas pressure sensors

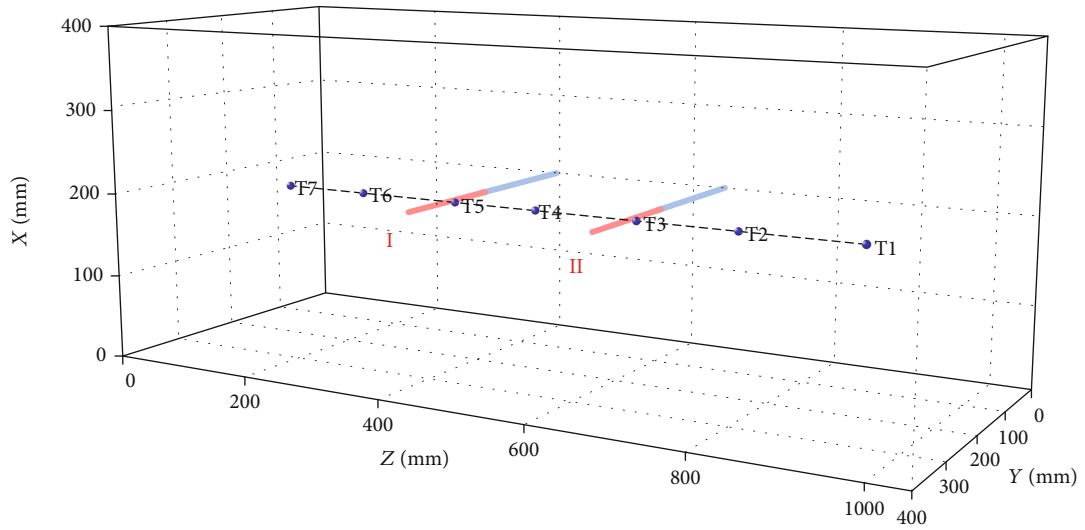

(b) Temperature sensors

Figure 1: Positions of gas pressure sensors and temperature sensors.

average which is a little larger than that of $P13$ and $P14$, as shown in Figure 3(b).

The gas pressure of 12 gas pressure sensors along the line $x = 200$ mm, $y = 250$ mm, and $z = 40$–1010 mm at different times are shown in Figure 3(c). It is apparent that the gas pressure at the drainage section of the borehole is always minimum at any time. The gas pressure at borehole I and borehole II is 0.57 MPa and 0.33 MPa after drainage of 1 min, respectively. However the gas pressure at other positions is still almost equal to the initial gas pressure. After gas drainage time of 8 h, the gas pressure at borehole I and borehole II is about 0.1 MPa and the gas pressure at other positions is approximately 0.03 MPa. That is, the decreasing rate of gas pressure reduces with the increase of distance from borehole and the difference between gas pressures at different positions decreases as the gas drainage progresses.

Gas desorption is an endothermic process that contributes to the drop in the coal temperature during gas drainage. Therefore, the variations of temperature at different positions are calculated and the curves of $\Delta T1$, $\Delta T2$, $\Delta T3$, and $\Delta T4$ are shown in Figure 4(a). We observe an overall trend of temperature drop similar to that of gas pressure during gas drainage: the fast and then slow drop rate in temperature and gas pressure. At the same time, the temperature sensor of $T3$, located near the middle of the drainage section of borehole, drops at the fastest rate during the whole drainage process with the final maximum drop of 12.5°C at last. The temperature sensor of $T1$, located farthest from borehole, drops at the slowest rate during the whole drainage process with a final minimum drop of 9.7°C. The temperature sensors of $T2$ and $T4$ are located at the same distance from borehole. However, the drop rate of $T4$ is faster than that of $T2$, especially after 90 mins of gas drainage. At last, the temperature drop of $T2$ is 11.8°C but the temperature drop of $T4$ is 12.4°C which is almost equal to that of $T3$.

The temperature drop curves of 7 temperature sensors along the line $x = 200$ mm, $y = 250$ mm, and $z = 152$–936 mm at different times are shown in Figure 4(b) showing

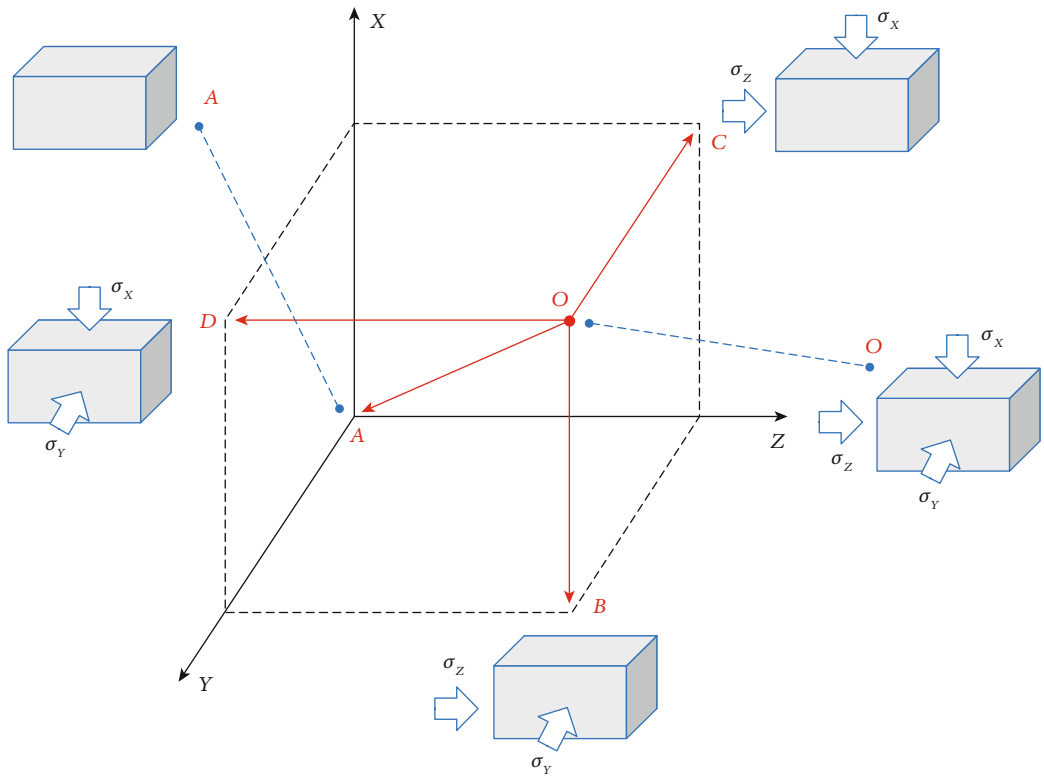

Figure 2: Unloading stress paths of pressure relief gas drainage experiments.

that the temperature of coal near boreholes drops fastest, followed by that between boreholes and far away from boreholes. As the gas drainage progresses, the temperature of coal between two boreholes (i.e., $T4$) is close to that near the boreholes, which indicates that two adjacent boreholes make the temperature of coal between borehole drop faster. This is mainly because that borehole interaction can accelerate the gas desorption of coal between boreholes and lead to the temperature of coal between boreholes declining faster [3].

Figure 5(a) shows the gas flow rate and gas production of different branch boreholes during gas drainage. The gas flow rate of borehole I (i.e., qI) has a maximum of 39.86 L/min at the beginning, then decreases with the gas drainage and finally drops to 0.45 L/min. Similarly, the gas flow rate of borehole II (i.e., qII) has a maximum of 40.78 L/min at the beginning, then decreases with gas drainage and finally drops to 0.35 L/min. However, the difference between gas production of borehole I (i.e., QI) and gas production of borehole II (i.e., QII) increases gradually with the process of gas drainage, then QI and QII reach 1285.34 L and 1219.43 L, respectively. The different drainage effects between two branch boreholes are mainly because of the incompletely homogeneous coal [31]. Therefore, the total gas flow rate and gas production of boreholes are critical, as shown in Figure 5(b). It can be seen that q (i.e., qI + qII) has the same evolution trend of qI and qII and Q (i.e., QI + QII) has the same evolution trend of QI and QII. The difference is that the peaks of q and Q are significant reaching 80.64 L/min and 2054.77 L, respectively.

3.2. Gas Flow Characteristics under Different Unloading Stress Paths. In order to study the influence of unloading stress paths on gas flow characteristics, gas pressure, or temperature at the same position during different experiments were compared together. Three types of sensor positions were chosen, namely, the position near boreholes, the position between boreholes, and the position far away from boreholes. The curves of $P25$, $P29$, and $P40$ during different experiments are shown in Figure 6. As can be seen from Figure 6(a), four curves have a sharp drop in the initial stage due to four gas pressure sensors that are close to borehole I. The curves of $P25$-XYZ and $P29$-Z almost coincide, and they are lower than the curve of $P25$-Y while the curve of $P25$-X remains the highest during the whole drainage process demonstrating that the unloading stress in the Z direction, and three directions has the most significant effect on gas pressure decline near the boreholes. The curves of $P29$ and $P40$ during different experiments have a similar evolution trend. $P29$ and $P40$ drop the fastest when unloading stress is in the three directions and drop the slowest when unloading stress in the Z direction. The impact of unloading stress in the X direction and Y direction on $P29$ and $P40$ is almost the same, as shown in Figures 6(b) and 6(c).

The curves of $\Delta T3$, $\Delta T4$, and $\Delta T6$ during different experiments are shown in Figure 7. As shown, coal temperature has the maximum descent when unloading stress is in the three directions and has the minimum descent when unloading stress is in the Z direction. $\Delta T3$ of unloading stress in X direction is bigger than that in Y direction when temperature sensors are near the borehole and are similar when temperature sensors are between boreholes and far away from

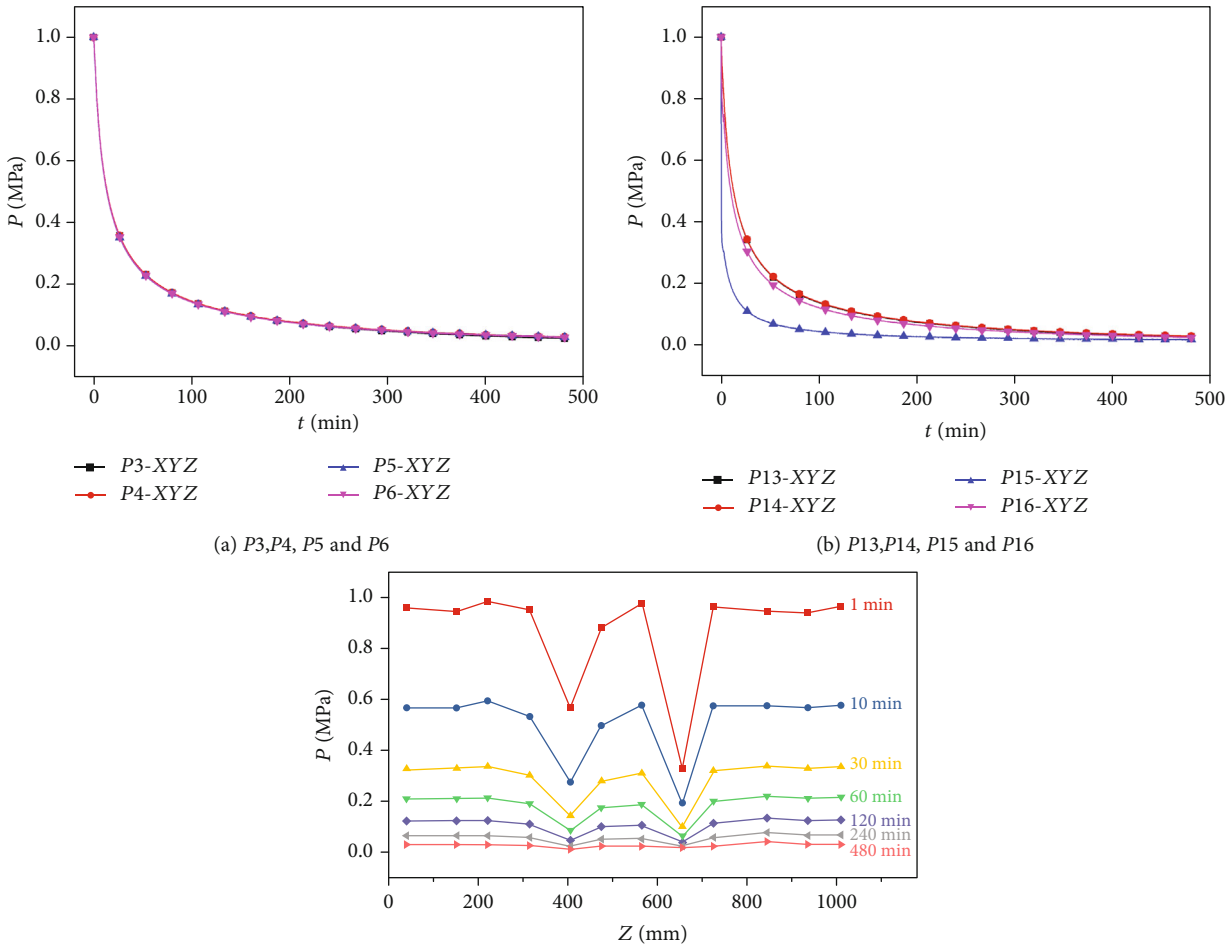

(a) *P*3,*P*4, *P*5 and *P*6

(b) *P*13,*P*14, *P*15 and *P*16

(c) $x = 200\ mm$, $y = 250\ mm$, $z = 40 - 1010\ mm$

Figure 3: Evolution of gas pressure during gas drainage.

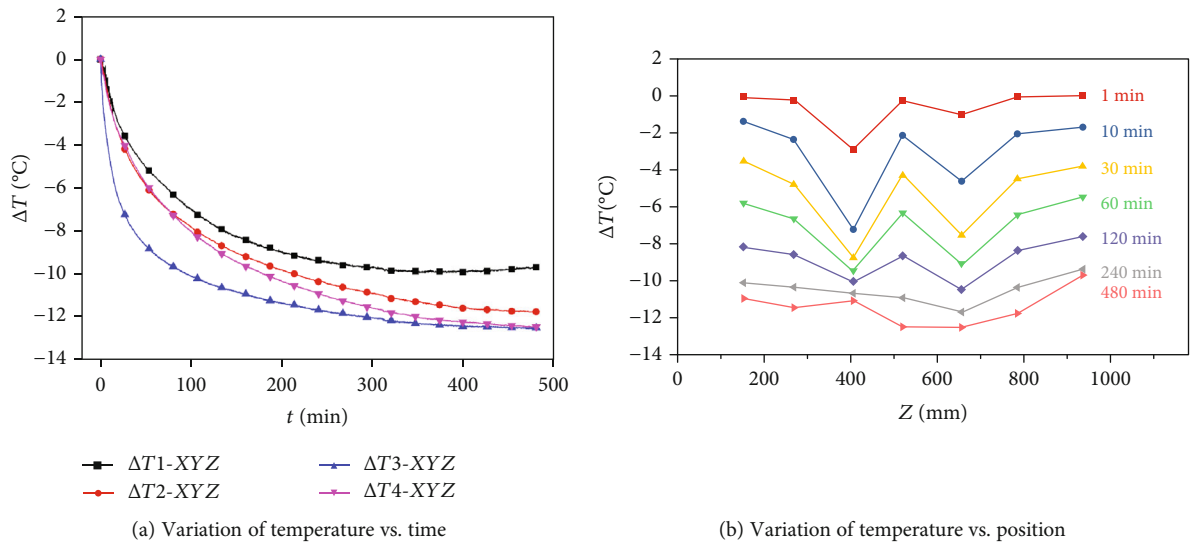

(a) Variation of temperature vs. time

(b) Variation of temperature vs. position

Figure 4: Evolution of coal temperature during gas drainage.

boreholes. In summary, gas flow characteristics are significantly affected by the unloading stress paths. Gas pressure and temperature have the maximum descent by unloading stress in the three directions and unloading stress of Z direction has the minimal impact only if the unloading stress is in one direction.

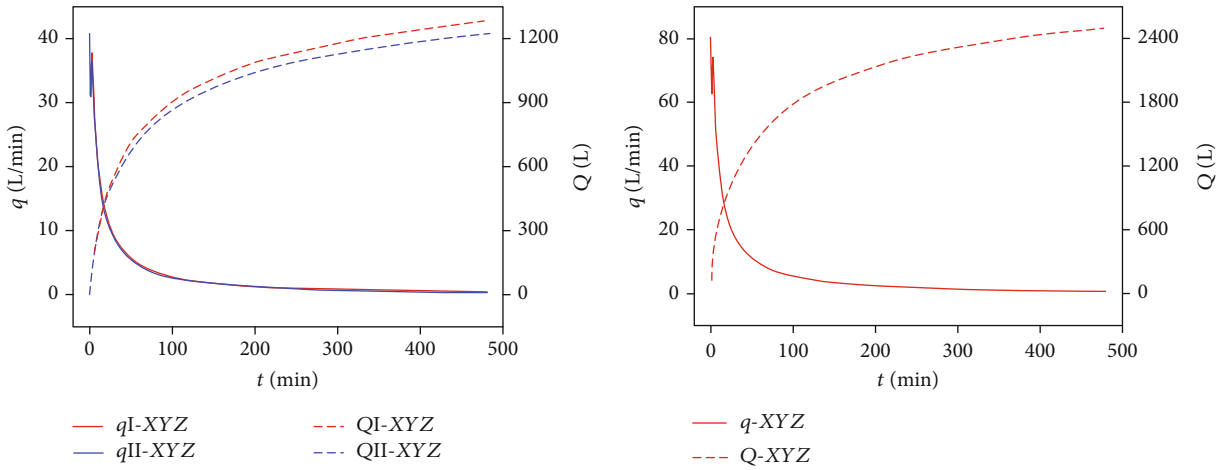

(a) Gas flow rate and gas production of different branch boreholes

(b) Total gas flow rate and gas production of two boreholes

Figure 5: Drainage effect of pressure relief gas drainage.

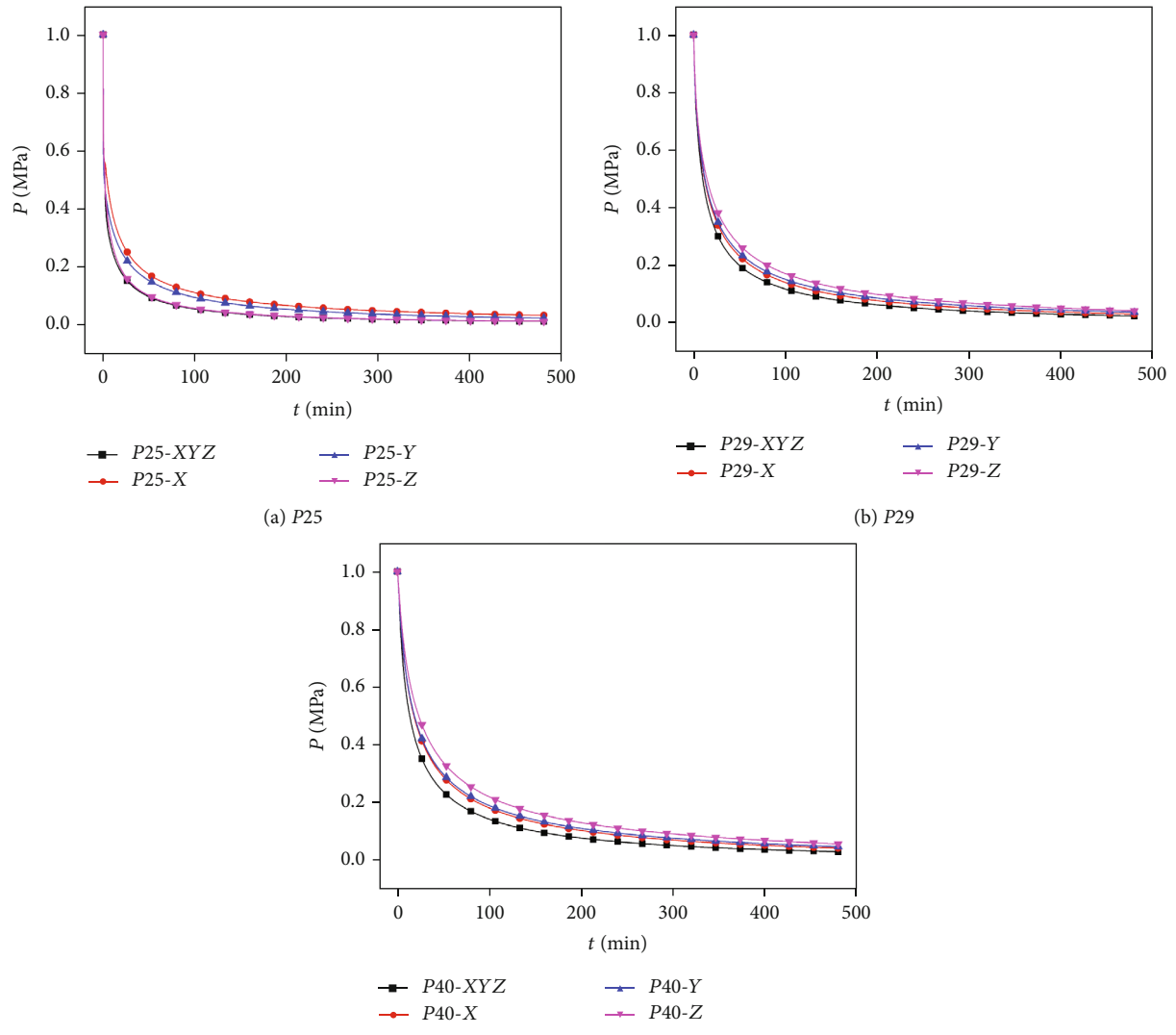

(a) *P25*

(b) *P29*

(c) *P40*

Figure 6: Evolution of gas pressure under different unloading stress paths.

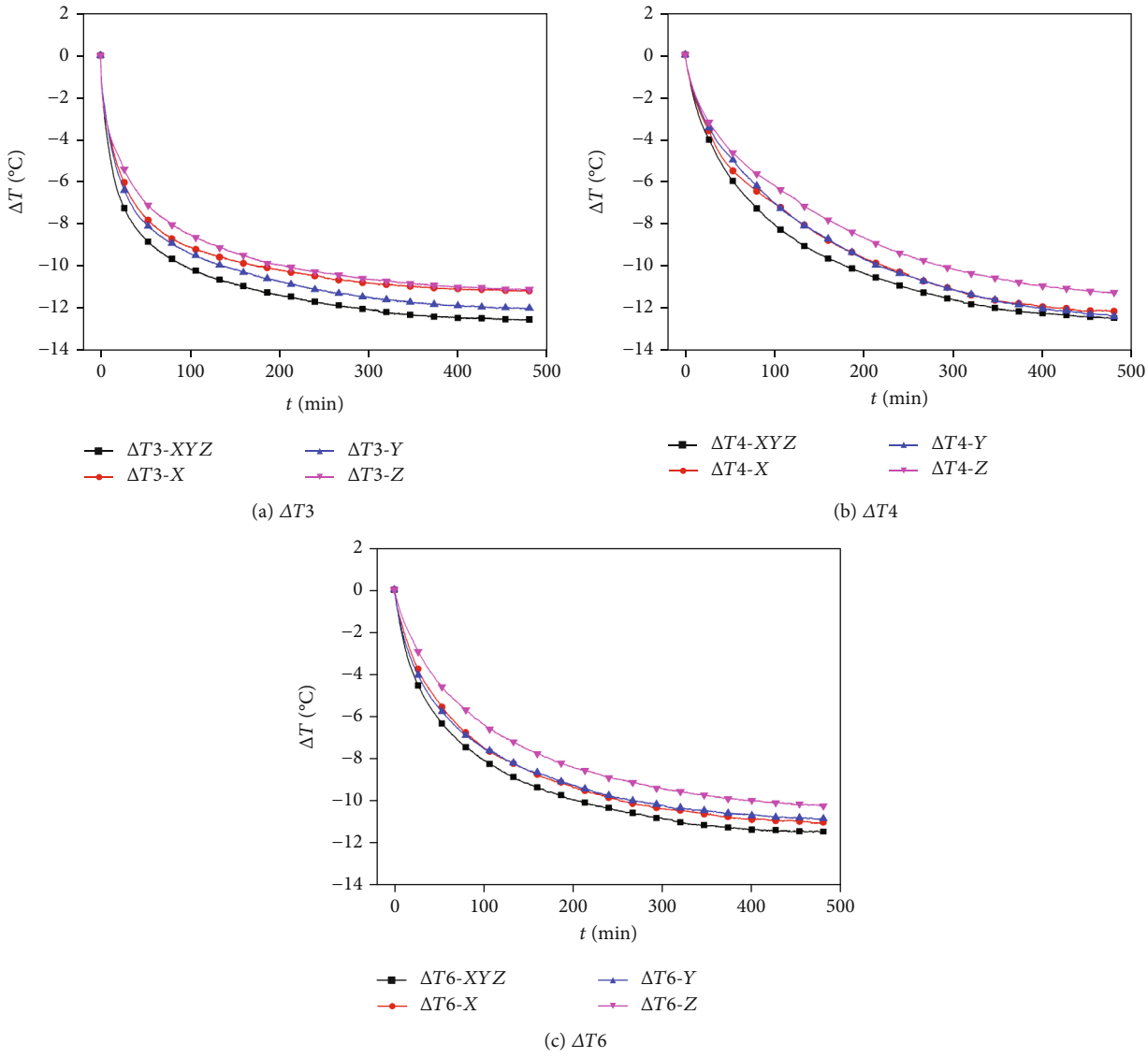

Figure 7: Variation of temperature under different unloading stress paths.

3.3. Gas Drainage Effect under Different Unloading Stress Paths. Total gas flow rate and gas production of two boreholes during different experiments are shown in Figure 8(a) demonstrating the impact of unloading stress paths on the gas drainage. Total gas flow rate peaks at the beginning of gas drainage and is 80.64 L/min, 80.54 L/min, 81.14 L/min, and 76.27 L/min with stress unloaded in three directions, namely, X direction, Y direction, and Z direction, respectively. The difference in the gas flow rates decreases gradually, which all have a minimum of 0.83 L/min after drainage of 8 h. Correspondingly, total gas production of four experiments are 2504.77 L, 2380.66 L, 2375.11 L, and 2287.00 L at last. It is apparent that the total gas production with stress unloaded in three directions is the highest and that with stress unloaded in Z direction is the lowest.

Total gas production is one of the key parameters indicating the gas drainage effect and the total gas production outputs at different drainage times with different unloading stress paths are compared further as shown in Figure 8(b). The total gas production outputs of the three different unloading stress paths are 1108.23 L, 992.18 L, 977.00 L, and 883.93 L after drainage of 30 mins. The total gas production with stress unloaded in three directions is the highest and serves as the control group and therefore the difference coefficient of gas production is defined below.

$$k = \frac{Q\text{-}i - Q\text{-}XYZ}{Q\text{-}XYZ} \times 100\% \; i = X, Y, Z, \tag{1}$$

Here, k is the difference coefficient of gas production.

The difference coefficients of the three experiments are -10.5%, -11.8%, and -20.2% after drainage of 30 mins indicating that the gas production declines when unloading stress in the Z direction is the largest. However, the difference coefficients of three experiments change to -7.3%, -8.2%, and -13.9% after drainage of 120 mins and finally change to -5.0%, -5.2%, and -8.7%. It is clear that the difference

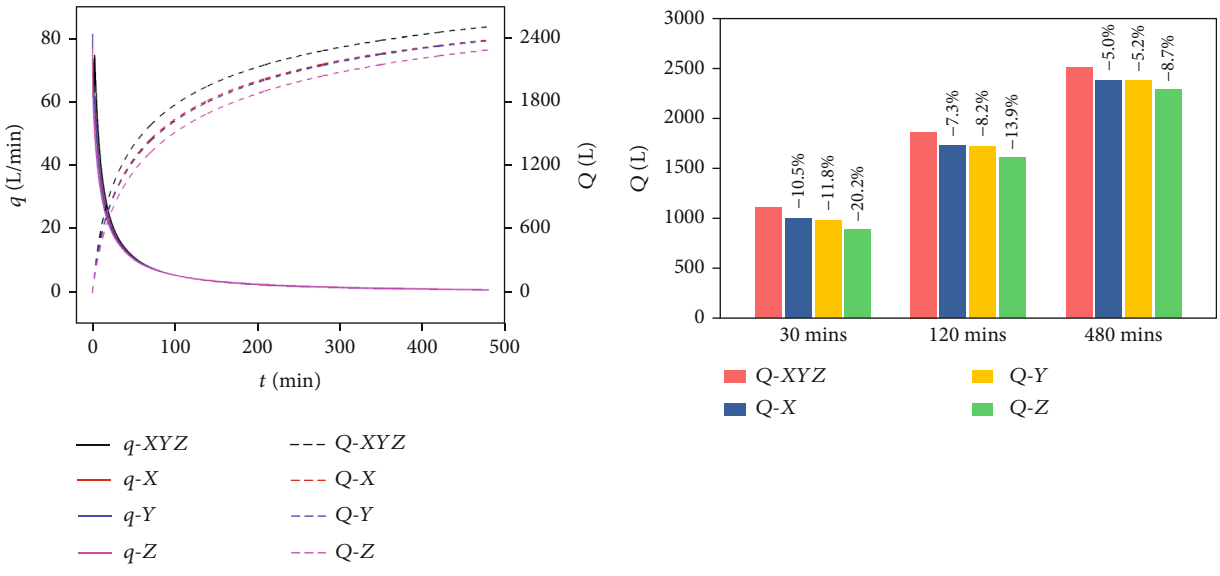

(a) Total gas flow rate and gas production vs. time

(b) Total gas production at 30 mins, 120 mins, and 480 mins

Figure 8: Total gas flow rate and gas production under different unloading stress paths.

coefficient of gas production is not only affected by unloading stress paths but also the drainage time.

3.4. Implication for Unloading Stress Path Selection. From the experimental results, the selection of unloading stress path is very important before pressure relief gas drainage, especially when only one direction of stress can be unloaded. Moreover, the effect of pressure relief gas drainage is controlled by unloading stress path and drainage time at the same time, as shown in Figure 9. From the evolution of three curves, we conclude that the gas production when unloading stress is in the Z direction has the largest drop followed by that when unloading stress is in the Y direction and then that when the unloading stress is in the X direction. That is to say, unloading stress in the three directions is the best unloading stress path, while unloading stress in the X direction is the best unloading stress path if only one direction of stress is chosen. Therefore, three directions of stress should be unloaded before pressure relief gas drainage to achieve the desired site conditions. Notably, it is possible that only one direction of stress can be unloaded considering the complex conditions, the difficulty, and long period of unloading stress.

Figure 9 shows that the evolution trends of the three curves are time dependent. The distribution area of the difference coefficient of gas production can be divided into three parts taking -5% and -10% as the demarcation points, namely, light green area, light yellow area, and light red area. The gas drainage effect can be considered to be approximately equal to that with three directions of stress unloaded in the light green area but they have a small gap in the light yellow area and a large gap in the light red area. As a result, the gas drainage effect in a single direction of stress unloaded is poor when conducting a short-term gas drainage (i.e., drainage period before line A) and the gas drainage effect in the X direction or Y direction of stress unloaded is feasible when conducting a medium-term gas drainage (i.e., drainage period between lines A and B) and the gas drainage effect in the Z direction of stress unloaded is satisfied only when conducting a long-term gas drainage (i.e., drainage period after line B).

In conclusion, the selection of unloading stress path before pressure relief gas drainage can be implemented as follows: Three directions of stress unloaded at the same time is the best selection of unloading stress path if conditions are favorable. The X direction of stress unloaded is the most suitable selection of unloading stress path if only one direction of stress is unloaded, followed by the Y direction of stress unloaded. The Z direction of stress unloaded is a viable selection of unloading stress path only for the long-term gas drainage.

4. Conclusions

Physical experiments of pressure relief gas drainage under different unloading stress paths were conducted using an LSMF device. Gas pressure, coal temperature, and gas flow rate were monitored during the whole drainage period. Gas pressure declines accompanied by a decrease in the coal temperature during drainage showed a similar evolution trend: dropping fast in the early stage and then declining slowly. At the same time, gas flow characteristics were significantly affected by unloading stress paths. Gas pressure and coal temperature had the maximum descent by simultaneously unloading stress in three directions and unloading stress of the Z direction had the minimal impact since only unloading was in one direction of stress. The influence of unloading stress paths on pressure relief gas drainage effect was time dependent, and the following conclusions are drawn: Three directions of stress unloaded is the best selection of unloading stress path if conditions permit. The X direction of stress unloaded is the best selection of unloading stress path if only one direction of stress can be unloaded, followed by the Y

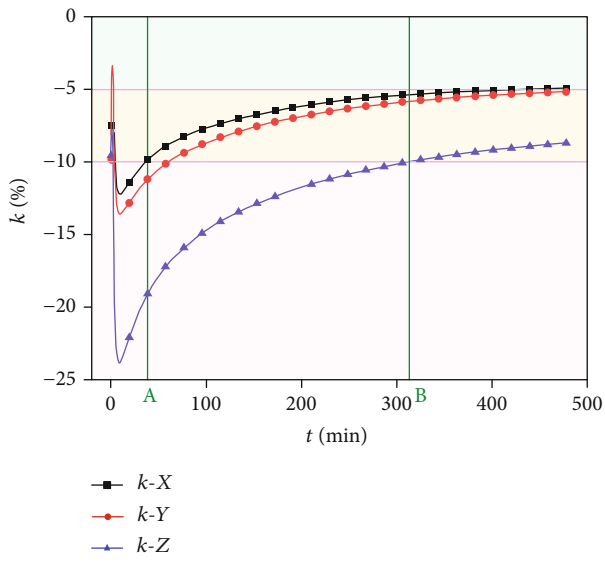

Figure 9: Difference coefficient of gas production under different unloading stress paths.

direction of stress unloaded. The Z direction of stress unloaded is a viable selection of unloading stress path only for the long-term gas drainage.

Data Availability

The data used to support the findings of this study are available from the corresponding author upon request.

Conflicts of Interest

The authors declare that there are no conflicts of interest regarding the publication of this study.

Acknowledgments

This work was supported by the National Natural Science Foundation of China (No. 51904293), the National Science and Technology Major Project of China (No. 2016ZX05044-002), the National Science Foundation of Jiangsu Province (No. BK20190627), and the China Postdoctoral Science Foundation (No. 2019M661998).

References

[1] M. Pillalamarry, S. Harpalani, and S. Liu, "Gas diffusion behavior of coal and its impact on production from coalbed methane reservoirs," *International Journal of Coal Geology*, vol. 86, no. 4, pp. 342–348, 2011.

[2] Y. Du, X. Chen, L. Li, and P. Wang, "Characteristics of methane desorption and diffusion in coal within a negative pressure environment," *Fuel*, vol. 217, pp. 111–121, 2018.

[3] C. Zhang, J. Xu, S. Peng, Q. Li, and F. Yan, "Experimental study of drainage radius considering borehole interaction based on 3D monitoring of gas pressure in coal," *Fuel*, vol. 239, pp. 955–963, 2019.

[4] L. Zhang, T. Ren, N. Aziz, and C. Zhang, "Evaluation of Coal Seam Gas Drainability for Outburst-Prone and High-CO2-Containing Coal Seam," *Geofluids*, vol. 2019, Article ID 3481834, 14 pages, 2019.

[5] G. Wang, Y. Liu, and J. Xu, "Short-term failure mechanism triggered by hydraulic fracturing," *Energy Science & Engineering*, vol. 8, no. 3, pp. 592–601, 2020.

[6] T. A. Moore, "Coalbed methane: A review," *International Journal of Coal Geology*, vol. 101, pp. 36–81, 2012.

[7] Q. Niu, L. Cao, S. Sang et al., "Study on the anisotropic permeability in different rank coals under influences of supercritical CO_2 adsorption and effective stress and its enlightenment for CO_2 enhance coalbed methane recovery," *Fuel*, vol. 262, article 116515, 2020.

[8] C. Ö. Karacan, F. A. Ruiz, M. Cotè, and S. Phipps, "Coal mine methane: A review of capture and utilization practices with benefits to mining safety and to greenhouse gas reduction," *International Journal of Coal Geology*, vol. 86, no. 2-3, pp. 121–156, 2011.

[9] S. A. Keim, K. D. Luxbacher, and M. Karmis, "A numerical study on optimization of multilateral horizontal wellbore patterns for coalbed methane production in Southern Shanxi Province, China," *International Journal of Coal Geology*, vol. 86, no. 4, pp. 306–317, 2011.

[10] Q. Li, J. Xu, F. Yan, S. Peng, C. Zhang, and X. Zhang, "Evolution characteristics of reservoir parameters during coalbed methane drainage via in-seam horizontal boreholes," *Powder Technology*, vol. 362, pp. 591–603, 2020.

[11] K. Jin, Y. Cheng, T. Ren et al., "Experimental investigation on the formation and transport mechanism of outburst coal-gas flow: Implications for the role of gas desorption in the development stage of outburst," *International Journal of Coal Geology*, vol. 194, pp. 45–58, 2018.

[12] G. Wang, P. Wang, Y. Guo, and W. Li, "A Novel True Triaxial Apparatus for Testing Shear Seepage in Gas-Solid Coupling Coal," *Geofluids*, vol. 2018, Article ID 2608435, 9 pages, 2018.

[13] Y. Gao, F. Gui, and A. Nieto, "A comparative study of gas explosion occurrences and causes in China and the United States," *International Journal of Mining, Reclamation and Environment*, vol. 30, no. 4, pp. 269–278, 2015.

[14] H. C. Lau, H. Li, and S. Huang, "Challenges and opportunities of coalbed methane development in China," *Energy & Fuels*, vol. 31, no. 5, pp. 4588–4602, 2017.

[15] C. Zhang, J. Xu, S. Peng, X. Zhang, X. Liu, and Y. Chen, "Dynamic Evolution of Coal Reservoir Parameters in CBM Extraction by Parallel Boreholes Along Coal Seam," *Transport in Porous Media*, vol. 124, no. 2, pp. 325–343, 2018.

[16] Y. Cheng, Y. Lu, Z. Ge, L. Cheng, J. Zheng, and W. Zhang, "Experimental study on crack propagation control and mechanism analysis of directional hydraulic fracturing," *Fuel*, vol. 218, pp. 316–324, 2018.

[17] C. Zhang, J. Xu, S. Peng, Q. Li, F. Yan, and Y. Chen, "Dynamic behavior of gas pressure and optimization of borehole length in stress relaxation zone during coalbed methane production," *Fuel*, vol. 233, pp. 816–824, 2018.

[18] T. Xia, F. Zhou, J. Liu, S. Hu, and Y. Liu, "A fully coupled coal deformation and compositional flow model for the control of the pre-mining coal seam gas extraction," *International Journal of Rock Mechanics and Mining Sciences*, vol. 72, pp. 138–148, 2014.

[19] L. Zhang, C. Zhang, S. Tu, H. Tu, and C. Wang, "A Study of Directional Permeability and Gas Injection to Flush Coal Seam Gas Testing Apparatus and Method," *Transport in Porous Media*, vol. 111, pp. 573–589, 2016.

[20] L. Yuan, "Theory of pressure relieved gas extraction and technique system of integrated coal production and gas extraction," *Journal of China Coal Society*, vol. 34, no. 1, pp. 1–8, 2009.

[21] C. Zhang, L. Zhang, S. H. Tu, D. Y. Hao, and T. Teng, "Experimental and numerical study of the influence of gas pressure on gas permeability in pressure relief gas drainage," *Transport in Porous Media*, vol. 124, no. 3, pp. 995–1015, 2018.

[22] C. Zhang, S. H. Tu, and L. Zhang, "Pressure-relief and methane production performance of pressure relief gas extraction technology in the longwall mining," *Journal of Geophysics and Engineering*, vol. 14, no. 1, pp. 77–89, 2017.

[23] G. Z. Yin, M. H. Li, C. B. Jiang, J. Xu, and W. P. Li, "Mechanical behavior and permeability evolution of gas infiltrated coals during protective layer mining," *International Journal of Rock Mechanics and Mining Sciences*, vol. 80, pp. 292–301, 2015.

[24] G. Z. Yin, H. Qin, and G. Huang, "Experimental study of characteristics of seepage and acoustic emission of gas-filled coal under different stress paths," *Chinese Journal of Rock Mechanics and Engineering*, vol. 32, no. 7, pp. 1315–1320, 2013.

[25] H. D. Chen, Y. P. Cheng, H. X. Zhou, and W. Li, "Damage and permeability development in coal during unloading," *Rock Mechanics and Rock Engineering*, vol. 46, no. 6, pp. 1377–1390, 2013.

[26] F. K. Wang, J. F. He, Y. P. Liang, Y. J. Luo, Z. W. Liao, and L. Li, "Study on the permeability characteristics of coal containing coalbed methane under different loading paths," *Energy Science & Engineering*, vol. 6, no. 5, pp. 475–483, 2018.

[27] Z. Shang, H. F. Wang, Y. P. Wang, B. Li, J. Dong, and Q. Q. Liu, "Optimal selection of coal seam pressure-relief gas extraction technologies: a typical case of the Panyi Coal Mine, Huainan coalfield, China," *Energy Sources, Part A: Recovery, Utilization, and Environmental Effects*, pp. 1–21, 2019.

[28] C. L. Zhang, J. Xu, G. Z. Yin, S. J. Peng, Q. X. Li, and Y. X. Chen, "A novel large-scale multifunctional apparatus to study the disaster dynamics and gas flow mechanism in coal Mines," *Rock Mechanics and Rock Engineering*, vol. 52, no. 8, pp. 2889–2898, 2019.

[29] L. Li, D. Z. Tang, Z. J. Pan, H. Xu, and L. L. Guo, "Evaluation of coalbed methane potential of different reservoirs in western Guizhou and eastern Yunnan, China," *Fuel*, vol. 139, pp. 257–267, 2015.

[30] G. Z. Yin, C. B. Jiang, J. G. Wang, J. Xu, D. M. Zhang, and G. Huang, "A New Experimental Apparatus for Coal and Gas Outburst Simulation," *Rock Mechanics and Rock Engineering*, vol. 49, no. 5, pp. 2005–2013, 2016.

[31] D. S. Yang, X. Y. Qi, W. Z. Chen, S. G. Wang, and F. Dai, "Numerical investigation on the coupled gas-solid behavior of coal using an improved anisotropic permeability model," *Journal of Natural Gas Science and Engineering*, vol. 34, pp. 226–235, 2016.